Molecular Crystals and Liquid Crystals
Publication details, including instructions for authors and subscription information:
http://www.tandfonline.com/loi/gmcl20

# Liquid Crystal/Polymer Composites: Kinetic Study of the Grating Formation in Holographic Polymer-Dispersed Liquid Crystals

Andreas Redler [a], Andreas Hoischen [a] & Heinz Kitzerow [a]
[a] Faculty of Science, Department of Chemistry, University of Paderborn, Warburger Straße, Paderborn, Germany

Version of record first published: 16 Jun 2011

To cite this article: Andreas Redler, Andreas Hoischen & Heinz Kitzerow (2011): Liquid Crystal/Polymer Composites: Kinetic Study of the Grating Formation in Holographic Polymer-Dispersed Liquid Crystals, Molecular Crystals and Liquid Crystals, 547:1, 97/[1787]-107/[1797]

To link to this article: http://dx.doi.org/10.1080/15421406.2011.572798

*Mol. Cryst. Liq. Cryst.*, Vol. 547: pp. 97/[1787]–107/[1797], 2011

ISSN: 1542-1406 print/1563-5287 online
DOI: 10.1080/15421406.2011.572798

Taylor & Francis
Taylor & Francis Group

# Liquid Crystal/Polymer Composites: Kinetic Study of the Grating Formation in Holographic Polymer-Dispersed Liquid Crystals

ANDREAS REDLER, ANDREAS HOISCHEN, AND HEINZ KITZEROW

Faculty of Science, Department of Chemistry, University of Paderborn, Warburger Straße, Paderborn, Germany



*Holographic polymer-dispersed liquid crystals are promising materials for switchable holograms, optical data storage, tunable beam deflectors and various diffractive optical elements, which can be addressed by electric fields. The present paper describes investigations on the grating formation in a model system. The results of holographic and calorimetric experiments are in good agreement with a reaction-diffusion model.*

**Keywords** Diffractive optical elements; holographic storage; polymer-dispersed liquid crystals; reaction-diffusion model

## 1. Introduction

Classical materials for the recording of holograms or holographic data storage are based on photosensitive inorganic compounds, such as silver bromide [1] or lithium niobate [2]. However, promising organic materials for these purposes have been developed during the last decades, for example reactive polymers for photographic films [3] or polymers combining photoconducting and electrooptic properties for photorefractive applications [4]. Copolymers or organic composites are particularly versatile with respect to the opportunities of molecular and structural design and the functional properties resulting thereof. The holographic formation of polymer-dispersed liquid crystals (PDLC) [5] provides the unique opportunity of fabricating holograms and diffractive optical elements whose diffraction efficiency can be modified by applying electric or magnetic fields [6]. Holographic polymer-dispersed liquid crystals (HPDLC) can be made either from photo-reactive mixtures by polymerization-induced phase separation [7] or from thermoplastic polymer composites by thermally induced phase separation [8]. In spite of the broad range of possible applications, comparisons of systematic experimental studies with theoretical models are scarce.

Address correspondence to Heinz Kitzerow, Faculty of Science, Department of Chemistry, University of Paderborn, Warburger Straße 100, 33098 Paderborn, Germany. Tel.: +49-5251 60 2156; Fax: +49-5251 60 4208; E-mail: Heinz.Kitzerow@upb.de

Typically, HPDLC samples are fabricated from a homogeneous mixture, which contains at least a non-reactive liquid crystal, a reactive monomer, and a photosensitive initiator. Eventually, sensitizing or plasticizing agents are added. Exposure of the sample to a holographic interference pattern leads to photo-polymerization in the positions of high radiation intensity, followed by diffusion of the monomer to these positions. Continued exposure leads to a phase separation of two phases where the concentrations of the polymer or the residual liquid crystal are enhanced, respectively. For irradiation with uniform intensity, the PDLC formation can be described by appropriate reaction-diffusion models [9]. In addition, models assuming a spatially periodic variation of the intensity have been developed [10–12]. However, the application of these models to specific materials is often based on assumptions about the reaction speed or the diffusion constants. Only recently, the results of kinetic measurements were incorporated in fundamental considerations [12]. In the present paper, we describe both photo-calorimetric and holographic studies of a model system, which is easy to handle. Measurements on the development of the diffraction efficiency are in good agreement with simulations based on a reaction-diffusion model.

## 2. Experimental Methods

Holographic photopolymerization was utilized to create one-dimensional gratings in a polymer-dispersed liquid crystal (PDLC) system containing 49 wt.% of the monomer trimethylolpropane triacrylate (TMPTA), 50 wt.% of the liquid crystal E7 and 1% of the photoinitiator Irgacure 784. The wide temperature range nematic mixture E7 (Merck, Darmstadt, Germany) consists of 51% 4-cyano-4′-pentylbiphenyl (5CB), 25% 4-cyano-4′-heptylbiphenyl (7CB), 16% 4-cyano-4′-octyloxybiphenyl (8OCB), and 8% 4-cyano-4′-pentylterphenyl (5CT). The mixture of the liquid crystal, the monomer TMPTA and the initiator was dissolved in dichloromethane. In order to get homogeneous samples, the solution was mixed in an ultrasonic bath. After evaporation of the solvent, the composition was used to fill the respective test cell (E.H.C. Japan, cell gap $d = 50\,\mu m$). The cells were exposed to the interference pattern of two laser beams to induce one-dimensional gratings.

The phase gratings (transmission holograms) were produced by splitting the collimated laser beam from a frequency doubled Nd:$YVO_4$ laser (532 nm) and focusing the resulting two beams on the sample (Fig. 1). The two laser beams have a power of about 0.85 mW each and are focused on a sample area of $0.2-0.56\,cm^2$, which yields an average intensity between 8.5 and $3\,mW/cm^2$. During exposure, the sample was also illuminated by a HeNe laser beam (633 nm) to monitor the diffraction efficiency during the grating formation. Figure 2 shows the resulting diffraction pattern of the induced one-dimensional grating.

In order to characterize the physical and chemical properties of the components, the refractive indices and the polymerization rates were measured in separate experiments. Table 1 contains the ordinary ($n_o$) and the extraordinary ($n_e$) refractive indices of E7 as well as the refractive indices of the monomer TMPTA and the respective polymer, which is formed in a radical reaction. These refractive indices were measured by means of a Leitz-Jelley-refractometer.

The photoreaction of both the pure monomer and the liquid crystal/monomer mixture was investigated by means of a modified apparatus made for differential scanning calorimetry (DSC). For these photo-DSC measurements, a DSC-2

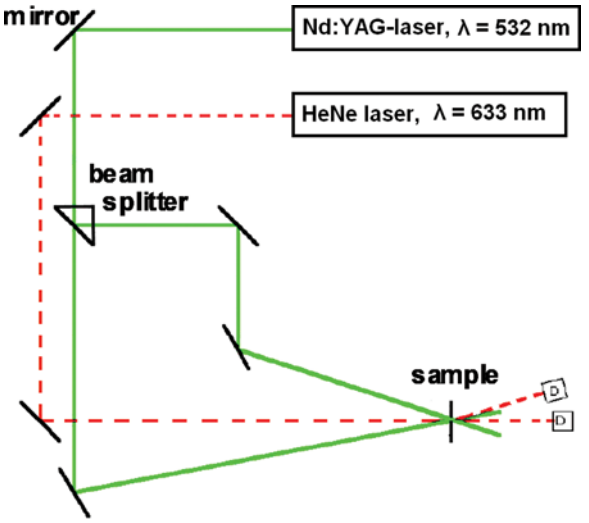


**Figure 1.** Holographic setup. The interference of two beams creates a one-dimensional grating, which in turn causes diffraction of the central incident beam. (Figure appears in color online.)

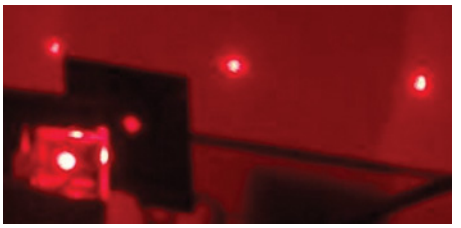

**Figure 2.** Diffraction pattern showing the 0th (center) and two 1st order diffraction spots. (Figure appears in color online.)

apparatus from Perkin-Elmer was equipped with an illumination unit (Fig. 3) and computer control, which provides access to measuring the heat of the photoreaction under similar conditions as in the laser experiment. More precisely, the sample was illuminated by green LEDs at a wavelength of 550 nm with an intensity of about $2\,mW/cm^2$. Further details are given in Ref. [13].

**Table 1.** Ordinary ($n_o$) and the extraordinary ($n_e$) refractive indices of the liquid crystal E7 and refractive indices of the TMPTA monomer as well as its corresponding polymer ($\lambda = 633$ nm)

| Liquid crystal E7 | | TMPTA | |
|---|---|---|---|
| $n_o$ | $n_e$ | $n_{(monomer)}$ | $n_{(polymer)}$ |
| 1.52531 | 1.75505 | 1.474 | 1.51389 |

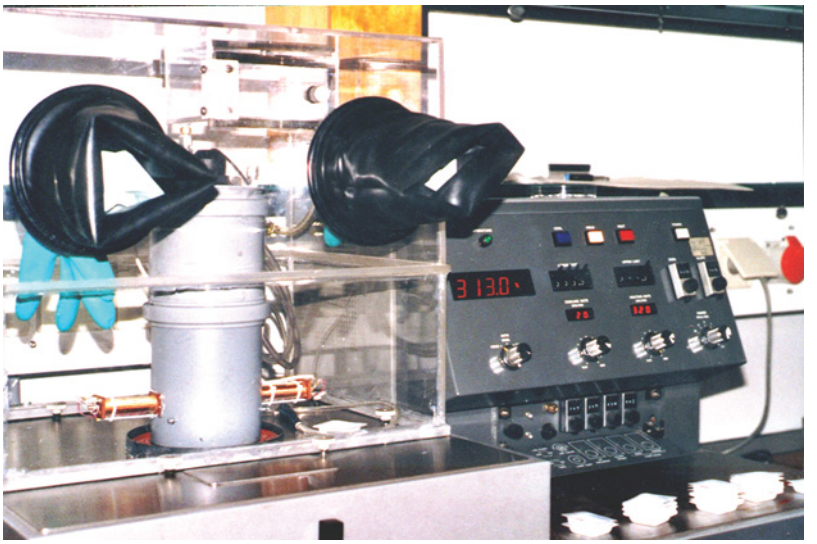

**Figure 3.** Photograph of the modified head of the photo-DSC, which makes it possible to measure the heat of photochemical reactions. The vertical tube to the left contains the light source and a computer controlled optical shutter for irradiation of the sample. The glove box is needed to investigate radical reactions in an oxygen-free environment. (Figure appears in color online.)

## 3. Results and Discussion

### 3.1. *Experimental Results*

The intensity $I_1$ of the 1st order diffraction spot was measured in order to determine the diffraction efficiency $\eta = I_1/I_0$ (Fig. 4), where $I_0$ is the intensity of the incident light.

Figure 5(a) represents the evolution of the diffraction efficiency of a grating, which was written with 8.5 mW/cm$^2$ at room temperature. In this case, the diffraction

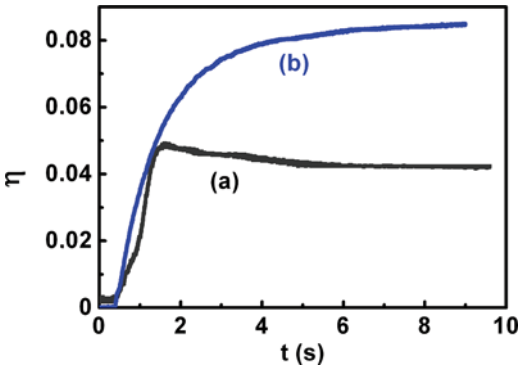


**Figure 4.** Diffraction efficiency versus time for the sample containing 49% TMPTA, 50% E7 and 1% Irgacure 784 at different irradiation intensities $I_0$. a) $I_0 = 8.5\,mW/cm^2$, b) $I_0 = 3\,mW/cm^2$. (Figure appears in color online.)

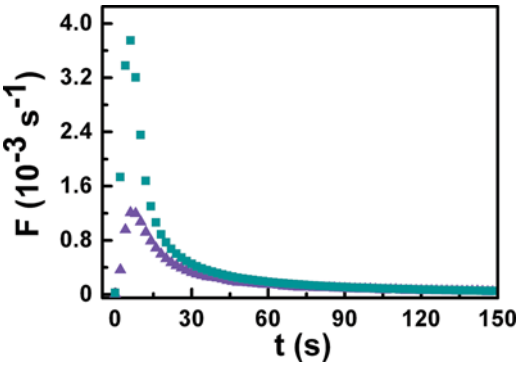


**Figure 5.** Polymerization rate R versus time for the pure monomers, cured at $T_{poly} = 313\,K$. (■) Tri-functional monomer TMPTA. (▲)Hexa-functional monomer Ebecryl 1290. (Figure appears in color online.)



efficiency shows a maximum, followed by a small decline to a saturation value. This unwanted decrease of the diffraction efficiency during the grating formation was also observed by other authors [14]. By varying the parameters of the irradiation, we found that the decrease of $\eta$ can be avoided if smaller intensities are used. For this purpose, the beam diameter was widened to 10 mm, so that the writing process of the grating was performed with an intensity of $3\,mW/cm^2$. The beam expansion results in a higher saturation value of the diffraction efficiency (Fig. 4(b)). The larger irradiance in Figure 4(a) implies that higher rates of reaction results in coalescence of the liquid crystal molecules to sizes large enough for random scattering [15,16].

The kinetics of the photo-polymerization reaction was studied using the photo-DSC equipment described above. Measurements of the heat of reaction versus time at constant temperature yield the time dependence of the polymerization rate. The squares in Figure 5 show the reaction rate of the pure monomer TMPTA versus time. After starting the irradiation, the reaction rate increases due to the increasing concentration of radicals. Later, the reaction rate decreases again, which can be attributed to the decreasing concentration and decreasing mobility of monomer molecules. Since the influence of the functionality, i.e., the number of photoreactive groups per monomer molecule was studied by other authors [10,17], we present the data for a hexa-functional compound, the urethane-based hexa-acrylate Ebecryl 1290 from the company UCB, for comparison (triangles in Fig. 5). Surprisingly, the maximum reaction speed of the hexa-functional compound Ebecryl 1290 is lower than the reaction speed of the tri-functional monomer TMPTA. Presumably, this result is caused by the higher viscosity of Ebecryl 1290.

However, this situation is reversed in the mixtures containing the liquid crystal and the respective monomer in a 1:1 ratio (Fig. 6). Here, the viscosities are more similar and mixtures containing a hexa-functional monomer polymerize faster than mixtures containing the tri-functional monomer TMPTA (Fig. 6(a)). The final degree of conversion of the tri-functional monomer is larger than that of the hexa-functional monomer, though (Fig. 6(b)). The quantitative values for the TMPTA/E7 mixture shown in Figure 6 are used to calculate the grating formation in this HPDLC mixture.

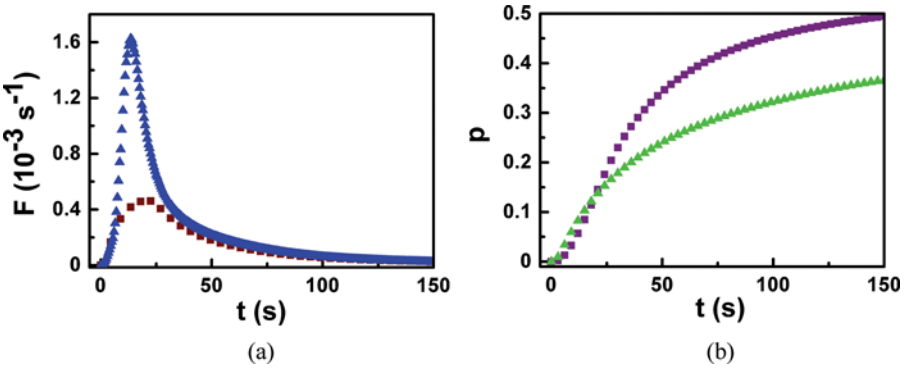


**Figure 6.** (a) Polymerization rate R and (b) degree of conversion p versus time for mixtures of the respective monomer (50%) and the liquid crystal E7 (50%). (■) Tri-functional monomer TMPTA. (▲) Hexa-functional monomer Ebecryl 1290. (Figure appears in color online.)

### 3.2. *Reaction-Diffusion Model*

The interference of two coherent laser beams leads to a non-uniform irradiance distribution. The rate of polymerization increases with increasing exposure intensity, i.e., in the bright regions more monomers per second disappear due to chemical reaction than in the dark regions. Thus, the position-dependent rate of polymerization leads to monomer concentration gradients and thus induces diffusion of monomers from the dark to the bright regions. The spatial variation of the concentrations of monomer, polymer and liquid crystal correspond to a spatial refractive index modulation, i.e., a phase grating.

A one-dimensional standard diffusion equation for the monomer concentration $u(x, t)$ can be written assuming that the monomers diffuse freely:

$$\frac{\partial u(x,t)}{\partial t} = \frac{\partial}{\partial x}\left[D(x,t)\,\frac{\partial u(x,t)}{\partial x}\right] - F(x,t)\,u(x,t), \tag{1}$$

In Eq. (1), the quantity $F(x, t)$ is the polymerization rate and $D(x, t)$ is the diffusion coefficient. The latter is not constant because of the change in polymer concentration and in the mobility of monomers.

The spatial distribution of the interference of two plane waves is given by

$$I(x,t) = I_0\,[1 + V(t)\,\cdot\cos(k\cdot x)]\,, \tag{2}$$

In Eq. (2), $I_0$ is the average irradiance, $V$ is the fringe visibility, and $k$ is given by $k = 2\pi/\Lambda$, with $\Lambda$ being the lattice constant. Assuming that the polymerization rate is proportional to the exposure irradiance, one can write

$$F(x,t) = F_0\,[1 + V(t)\cdot\cos(k\cdot x)]\,. \tag{3}$$

For our numerical calculations, we applied a method which was developed by Zhao and Mouroulis [18] and extended by other authors [19,20]. Because of the periodic character of the monomer concentration, the solutions of Eq. (1) can be expanded

in a Fourier series. After substituting the quantity $F(x, t)$ in Eq. (1) by a Fourier series and separating the different harmonics, a coupled set of differential equations is obtained [18]. Considering only the amplitudes $u_i(\tau)$ of the leading Fourier terms ($i = 0, 1, 2, 3$) of the monomer concentration yields four coupled differential equations:

$$\frac{du_0(\tau)}{d\tau} = -u_0(\tau) - \frac{1}{2} V u_1(\tau), \tag{4}$$

$$\frac{du_1(\tau)}{d\tau} = -V u_0(\tau) - [1 + R\ \exp(-\alpha\tau)\ \cosh(\alpha V\tau)]\ u_1(\tau) - \left[\frac{1}{2} V - R\ \exp(-\alpha\tau)\ \sinh(\alpha V\tau)\right] u_2(\tau), \tag{5}$$

$$\frac{du_2(\tau)}{d\tau} = -\left[\frac{1}{2} V - R\ \exp(-\alpha\tau)\ \sinh(\alpha V\tau)\right] u_1(\tau) - [1 + 4R\ \exp(-\alpha\tau)\ \cosh(\alpha V\tau)]\ u_2(\tau) - \left[\frac{1}{2} V - 3R\ \exp(-\alpha\tau)\ \sinh(\alpha V\tau)\right] u_3(\tau), \tag{6}$$

$$\frac{du_3(\tau)}{d\tau} = -\left[\frac{1}{2} V - R\ \exp(-\alpha\tau)\ \sinh(\alpha V\tau)\right] u_2(\tau) - [1 + 9R\ \exp(-\alpha\tau)\ \cosh(\alpha V\tau)]\ u_3(\tau), \tag{7}$$

Where the parameter $R = D_a k^2/F_0$ describes the ratio of the diffusion rate $D_a k^2$ and polymerization rate $F_0$, with $D_a$ being the initial diffusion coefficient, and the quantity $\tau = F_0 t$ is a reduced time. The concentration of polymerized monomers after an exposure time $t$ is

$$N(x, t) = \int_0^t F(x, t')\, u(x, t')\, dt'. \tag{8}$$

In our simulation, Eqs. (4)–(8) are solved numerically using Mathcad [21] in order to determine the position- and time-dependent concentrations of polymer and monomer. The distribution of the liquid crystal concentration $\Phi_{LC}$ is controlled by local mass conservation and can be expressed as

$$\Phi_{LC}(x, t) = 1 - u(x, t) - N(x, t). \tag{9}$$

The refractive index profile is given by [10]

$$n(x, t) = \langle n_{LC} \rangle\, \Phi_{LC}(x, t) + n_p\, N(x, t) + n_m\, u(x, t), \tag{10}$$

where $n_m$ and $n_p$ are, the monomer and polymer refractive indices, respectively. The average refractive index $<n_{LC}>$is given by

$$<n_{LC}> = [(2n_0^2 + n_e^2)/3]^{1/2}. \tag{11}$$

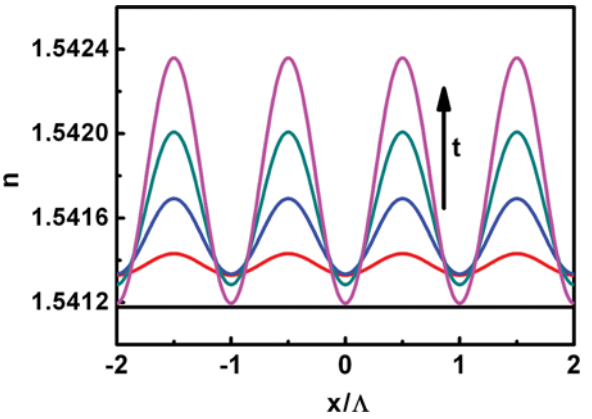


**Figure 7.** Evolution of the spatial distribution of the refractive index during the polymerization process.

Figure 7 shows the spatial and temporal behavior of the refractive index, which was obtained by solving the differential Eqs. (4)–(8) and inserting the numerical results in Eq. (10).

The diffraction properties of the induced grating can be described by the diffraction efficiency, which is defined as the ratio of the 1st order diffracted light intensity and the incident intensity $\eta = I_1/I_0$. The details of the diffraction pattern depend on the parameter

$$Q = 2\pi\,\lambda\,d/n\,\Lambda^2 \tag{12}$$

(which was first introduced in order to describe the optical diffraction induced by sound waves [22]. This parameter changes with the sample thickness d. A grating can be regarded as a volume grating when the condition $Q >> 1$ holds. Kogelnik's coupled wave theory [23] gives good results for values of $Q \geq 10$. Small values ($Q << 1$) correspond to the thin gratings that are described by the diffraction theory developed by Raman and Nath [22]. For our experiments, the lattice constant $\Lambda = 4\,\mu m$ and the wavelength $\lambda = 0.633\,\mu m$ result in a value of $Q \approx 8$, which is at the borderline between the two regimes described in Refs. [22,23].

For the volume grating, the diffraction efficiency $\eta_1$ can be calculated using the coupled wave theory expression for a sinusoidal grating [23,24]:

$$\eta_1 = \sin^2\left(\frac{\pi\,\delta n\,d}{\lambda\,\cos\theta}\right), \tag{13}$$

where $\delta n$ is the amplitude of the refractive index modulation, $d$ is the grating thickness, $\lambda$ is the wavelength of the incident beam, and $\theta$ is the angle of light incidence. In the Raman-Nath regime, the diffraction efficiency can be calculated by [23]

$$\eta_2 = J_1^2\left(\frac{2\pi\,\delta n\,d}{\lambda}\right) = \left\{\sum_{r=0}^{\infty}\frac{(-1)^r}{r!\;\Gamma(r+2)}\cdot\left(\frac{\pi\,\delta n\,d}{\lambda}\right)^{2r+1}\right\}^2, \tag{14}$$

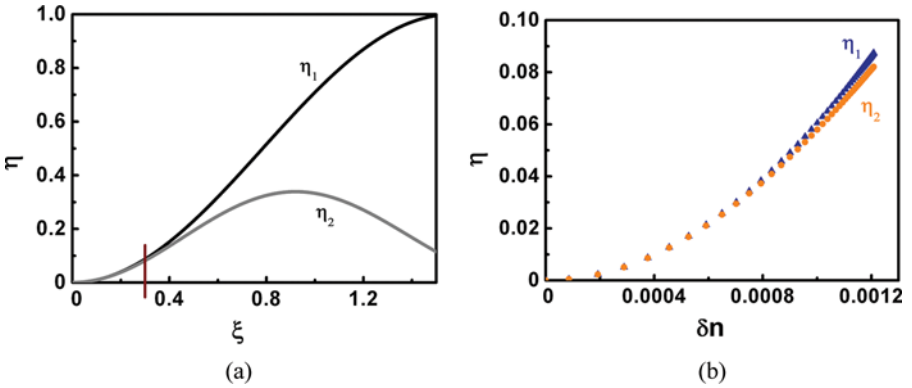


**Figure 8.** Theoretical diffraction efficiencies $\eta_1$ of a thick grating [Eq. (12)] and $\eta_2$ of a thin grating [Eq. (13)]. (a) $\eta_1$ and $\eta_2$ plotted as a function of the parameter $\xi = (\pi \cdot d \cdot \delta n)/\lambda$. (b) $\eta_1$ and $\eta_2$ plotted as a function of the refractive index modulation $\delta n$. The vertical line indicates the saturation value of the diffraction efficiency, calculated for our experimental parameters. (Figure appears in color online.)

where $J_1$ is the Bessel function of the 1st order and $\Gamma$ is the Gamma function. The diffraction efficiencies given by Eqs. (13) and (14) can be described as a function of $\xi = (\pi \cdot d \cdot \delta n)/\lambda$. In Figure 8, the quantities $\eta_1$ and $\eta_2$ given by Eq. (13) and Eq. (14) are plotted as a function of $\xi$ (Fig. 8(a)) and of $\delta n$ (Fig. 8(b)), respectively. Figure 8(a) shows the general shape of the functions $\eta_1(\xi)$ and $\eta_2(\xi)$ given by Eqs. (13) and (14), although the respective expressions are valid only in the limit of small values of $\xi$. The maximum value of $\xi$ corresponding to our experiments is indicated by a vertical line ($\xi_{max} \approx 0.3$). Figure 8(b) shows more clearly the appreciable differences between $\eta_1$ and $\eta_2$ in the relevant interval of $\delta n$ values. For the parameters studied experimentally, the approximation $\xi < 1$ is clearly valid.

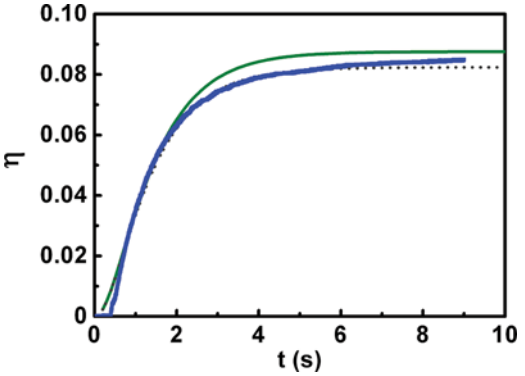


**Figure 9.** Development of the diffraction efficiency $\eta$: Comparison of the experimental results and the simulations. (o) Experimental values for the sample containing 49% TMPTA, 50% E7 and 1% Irgacure 784 [as represented in Fig. 4(b)]. Solid line: Theoretical values $\eta_1$ expected for a thick grating. Dotted line: Theoretical values $\eta_2$ expected for a thin grating. (Figure appears in color online.)

Figure 9 shows the simulated diffraction efficiencies, which were obtained from Eqs. (13) and (14) after inserting the numerical solutions of the coupled differential Eqs. (4)–(7) in the Eqs. (8)–(10) with the assumption of $D_a = 5 \cdot 10^{-12}\,cm^2/s$. As expected, the saturation value of the diffraction efficiency $\eta_1$ for an ideal volume grating (solid line) is slightly larger than the value $\eta_2$ of an ideal thin grating (dotted line). However, the expected influence of the sample thickness on this saturation value is not dramatic. For comparison, the experimental data points given in Figure 4(b) are also presented in Figure 9. The initial development of the grating is obviously very well described by inserting the experimental polymerization rates in the model developed by Zhao and Mouroulis [18–20]. As expected for $Q \approx 8$, the saturation values of the diffraction efficiency observed experimentally are between the two theoretical values expected for a thin grating [22] and a volume grating [23], respectively.



## 4. Conclusions and Perspectives

In conclusion, the present study shows that one can simulate the development of the diffraction efficiency $\eta(t)$ during the formation of a one-dimensional HPDLC grating from experimental data of the refractive indices of the individual HPDLC components (Table 1) and the polymerization rates in the HPDLC mixtures (Fig. 6). The theoretical $\eta(t)$ curves calculated using an estimated value of the diffusion constant fit the experimental diffraction data very well.

However, our photo-DSC measurements (Figs. 5 and 6) indicate that photocalorimetric data can be used only if they are obtained from a mixture having the same composition as the initial HPDLC sample. In addition to the number of reactive groups of the monomer [16], the viscosity has a crucial influence on the polymerization rate. It should be emphasized that the pure hexa-functional monomer shows a lower reaction rate than the tri-functional monomer (Fig. 5). This counterintuitive finding can be attributed to the high viscosity of the hexafunctional monomer. Only if the respective monomer is diluted by the liquid crystal, the situation is reversed (Fig. 6). This example demonstrates that the simulation of complex reaction diffusion systems – like HPDLC – requires experimental data, which have been measured under conditions which are very similar to the HPDLC experiment to be simulated.

To complete this study, it is therefore desirable to measure also the diffusion constants of the components in an HPDLC mixture. Such measurements are currently under consideration.

## Acknowledgment

The authors would like to thank the company UCB for providing the hexa-functional monomer Ebecryl 1290. Financial support by the German Research Foundation (GRK 1464) is gratefully acknowledged.

## References

[1] Lietze, E. (1888). *Modern Heliographic Processes: a Manual of Instruction in the Art of Reproducing Drawings, Engravings, Manuscripts, etc., by the Action of Light; for the*

*Use of Engineers, Architects, Draughtsmen, Artists, and Scientists*, Van Nostrand, D. (Ed.), reprinted by Cambridge Scholars Publishing: New York, (2010).
[2] Frejlich, J. (2007). *Photorefractive Materials: Fundamental Concepts, Holographic Recording and Materials Characterization*, John Wiley & Sons: Hoboken, NJ, USA.
[3] Rhee, U.-S., Caulfield, H. J., Vikram, C. S., & Shamir, J. (1995). *Appl. Opt.*, *34*, 846.
[4] Bernard Kippelen, (2007). *Photorefractive Materials and Their Applications 2*, Günter, P. & Huignard, J.-P. (Eds.), Chapter 14 (*Organic Photorefractive Materials and Their Applications*), Springer Series in Optical Sciences, Springer: New York, Vol. 114, 487.
[5] Drzaic, P. S. (1995). *Liquid Crystal Dispersions*, World Scientific: Singapore.
[6] Tondiglia, V. P., Natarajan, L. V., Sutherland, R. L., Bunning, T. J., & Adams, W. W. (1995). *Opt. Lett.*, *20*, 1325.
[7] Margerum, J. D., Lackner, A. M., Ramos, E., Smith, G. W., Vaz, N. A., Kohler, J. L., & Allison, C. R. (March 17, 1992). *Polymer dispersed liquid crystal film devices*, U.S. patent 5,096,282.
[8] Kitzerow, H.-S., Strauß, J., & Jain, S. C. (1996). *Proc. SPIE*, *2651*, 80.
[9] Serbutoviez, C., Kloosterboer, J. G., Boots, H. M. J., & Touwslager, F. J. (1996). *Macromolecules*, *29*, 7690.
[10] Bowley, C. C., & Crawford, G. P. (2000). *Appl. Phys. Lett.*, *76*(16), 2235.
[11] Meng, S., Kyu, T., Natarajan, L. V., Tondiglia, V. P., Sutherland, R. L., & Bunning, T. J. (2005). *Macromolecules*, *38*, 4844.
[12] Meng, S., Duran, H., Hu, J., Kyu, T., Natarajan, L. V., Tondiglia, V. P., Sutherland, R. L., & Bunning, T. J. (2007). *Macromolecules*, *40*, 3190.
[13] Hoischen, A. (2005). Ph.D. thesis, University of Paderborn.
[14] Shim, S. S., Cho, Y. H., Yoon, J. H., & Kim, B. K. (2009). *European Polymer Journal*, *45*, 2184.
[15] Bunning, T. J., Natarajan, L. V., Tondiglia, V. P., & Sutherland, R. L. (2000). *Annu. Rev. Mater. Sci.*, *30*, 83.
[16] Sarkar, M. D., Gill, N. L., Whitehead, B., & Crawford, G. P. (2003). *Macromolecules*, *36*, 630.
[17] Bunning, T. J., Natarajan, L. V., Tondiglia, V. P., Dougherty, G., & Sutherland, R. L. (1997). *J. Polym. Sci.: Part B: Polymer Physics*, *35*, 2825.
[18] Zhao, G., & Mouroulis, P. (1994). *Journal of Modern Optics*, *41*, 1929.
[19] Colvin, V. L., Larson, R. G., Harris, A. L., & Schilling, M. L. (1997). *J. Appl. Phys.*, *81*, 5913.
[20] Oh, H., Lee, H., Kim, E., Do, D. D., & Kim, N. (2006). *Organic Holographic Materials and Applications IV, Proc. SPIE, 6335, 1*, San Diego: CA, USA.
[21] Software (2001). *Mathcad*, Student Edition 2001, Mathsoft company.
[22] Raman, C. V., & Nath, N. S. N. (1935). *Proc. Indian Acad. Sci.*, *2*, 406.
[23] Kogelnik, H. (1969). *Bell System Tech. Journal*, *48*, 2909.
[24] Yeh, P. (1993). *Introduction to Photorefractive Nonlinear Optics*, 1st ed., Wiley: New York.